NASA-TM-87687 19860021598

NASA Technical Memorandum 87687

USAAVSCOM TECHNICAL REPORT 86-B-1

AEROELASTIC CONSIDERATIONS FOR TORSIONALLY SOFT ROTORS

WAYNE R. MANTAY AND
WILLIAM T. YEAGER, JR.

AUGUST 1986

NASA
National Aeronautics and
Space Administration

Langley Research Center
Hampton, Virginia 23665

AEROELASTIC CONSIDERATIONS FOR TORSIONALLY SOFT ROTORS

Wayne R. Mantay & William T. Yeager, Jr.
NASA/Langley Research Center
Army Structures Laboratory
Hampton, Virginia

Abstract

A research study was initiated to systematically determine the impact of selected blade tip geometric parameters on conformable rotor performance and loads characteristics. The model articulated rotors included baseline and torsionally soft blades with interchangeable tips. Seven blade tip designs were evaluated on the baseline rotor and six tip designs were tested on the torsionally soft blades. The designs incorporated a systematic variation in geometric parameters including sweep, taper, and anhedral. The rotors were evaluated in the NASA Langley Transonic Dynamics Tunnel at several advance ratios, lift and propulsive force values, and tip Mach numbers. A track sensitivity study was also conducted at several advance ratios for both rotors. Based on the test results, tip parameter variations generated significant rotor performance and loads differences for both baseline and torsionally soft blades. Azimuthal variation of elastic twist generated by variations in the tip parameters strongly correlated with rotor performance and loads, but the magnitude of advancing blade elastic twist did not. In addition, fixed system vibratory loads and rotor track for potential conformable rotor candidates appears very sensitive to parametric rotor changes.

Introduction

Reducing helicopter vibratory loads while improving performance through passive control has been the goal of the Aeroelastically Conformable Rotor (ACR) concept. Initial ACR studies (ref. 1) examined the potential of a conformable rotor to alter the unfavorable blade spanwise and azimuthal load distributions which lead to increased vibratory bending loads and power requirements. Those test results on a model hingeless rotor indicated that elastic twist measurably changed blade loads on a torsionally soft blade. The incorporation of time varying elastic twist, as a promising method of achieving a passive control concept, has been identified analytically (ref. 2). Blade design features producing that desired elastic control were suggested in reference 2 for an articulated rotor.

The effect of blade tip shape on rotor performance and loads has received much attention for application to multi-bladed helicopters (refs. 3-5). Experimental data have also been obtained (ref. 6) which initiated identification of blade tip shape as a promising passive control concept. The reference 6 test utilized a model rotor blade with conventional torsional stiffness, and while the resulting loads and performance of the configurations were tip-shape-dependent, the identification of which parameter caused each load or performance change was elusive. This was due, in part, to multiple parameter variations occurring with each tip change. Nevertheless, the concept of passive control to achieve better rotor performance while reducing loads was encouraged by these results and several conformable designs were pursued. The resulting studies (refs. 7-8) considered variations in blade torsional stiffness, airfoil section, mass distribution, and trailing edge tab deflection, as well as tip geometry, in the design. The wind-tunnel tests of these ACR concepts produced encouraging loads and performance data, but the aeroelastic mechanism for design success or failure was not obvious.

Expanded testing and analysis of the configurations of reference 6 resulted in identification of several key issues for future ACR application and development (ref. 9). For the baseline torsionally stiff rotor used in that test, the parametric variations of tip sweep, taper and anhedral did measurably change the elastic twist and integrated performance, but there did not appear to be a strong connection between elastic twist and performance. Additional tests on the blades of reference 8 which incorporated large tip spans and trailing edge tab deflections (refs. 10-11) showed performance and loads variations which were not easily explainable by individual parameter effects.

The parameters most effective in improving conformable rotor performance and loads characteristics have thus not been systematically determined. Although it has been shown that changes in adjustable trailing edge tabs have significant effects on conformable rotor behavior (ref. 11), the rotor blade tip operates in a very influential portion of the rotor disk and thus provides significant research impetus. This is especially true if ACR success is dependent on elastic twist control. Consequently, the research study described herein was initiated to systematically determine the effect of selected blade tip geometric parameters on ACR performance and loads characteristics. This data is presented for advance ratios of .35 and .40 at one rotational tip Mach number.

In addition, the utilization of a conformable rotor concept should be evaluated not only for the measure of success with which it achieves its performance and loads goals, but also how well it can be "fielded." That is how much change, if any, in current installation and rotor tuning is necessary for the new rotor concept to be employed. Rotor control sensitivity is an example of such a concern (ref. 11). Another aspect of this

transition for the conformable rotor is rotor tracking characteristics and the implications for rotor and fuselage loads. Initial results from the present study (ref. 12) provided some insight into the mechanisms involved in conformable rotor behavior. The results of the completed test program are included here.

Notation

a speed of sound, ft/sec

b number of blades

C_D rotor drag coefficient, $\frac{D}{\rho\pi R^2(\Omega R)^2}$

C_L rotor lift coefficient, $\frac{L}{\rho\pi R^2(\Omega R)^2}$

$\bar{C}_L$ rotor mean lift coefficient

C_Q rotor torque coefficient, $\frac{Q}{\rho\pi R^3(\Omega R)^2}$

c blade chord, in.

c.g. measured section center of gravity location, in.

a.c. computed section aerodynamic center location, in.

D rotor drag, lb.

H rotor force perpendicular to control axis, lb.

$I_{1/4_c}$ blade tip torsional mass inertia about 1/4 chord (ft-lb-sec^2)

I_θ blade section torsional mass inertia per foot about pitch axis (lb-sec^2)

L rotor lift, lb.

M_T rotor blade tip Mach number, $\frac{\Omega R}{a}$

Q rotor torque, ft-lb.

r blade radial station, ft.

R rotor radius, ft.

V free-stream velocity, ft/sec

α_s angle of attack of rotor shaft, positive tilt aft, deg.

$\Delta\theta_1$ elastic twist angle, positive nose-up, deg.

μ rotor advance ratio, $\frac{V}{\Omega R}$

ρ mass density of test medium, slug/ft3

σ nominal rotor solidity ratio, $bc/\pi R$ = .082

ψ azimuth angle of rotor blade, deg

Ω rotor rotational speed, rad/sec

ω natural frequency of rotating blade, rad/sec

Abbreviations

R rectangular
S sweep
T tapered
A anhedral

Apparatus

Wind Tunnel

The experimental program was conducted in the Langley Transonic Dynamics Tunnel (TDT) shown in figure 1. The TDT is a continuous flow tunnel with a slotted test section and is capable of operation up to Mach 1.2 at stagnation pressures up to 1 atm. The tunnel test section is 16 ft square with cropped corners and has a cross-sectional area of 248 ft^2. Either air or Freon-12[1] may be used as a test medium in the TDT. Because of its high density and low speed of sound, the use of Freon-12 aids the matching of full-scale Reynolds number and Mach number to model-scale values. Also, some restrictions on model structural design are eased, while dynamic similarity is still maintained. The heavier test medium permits a simplified structural design to obtain the required stiffness characteristics and thus eases the design and/or fabrication requirements of the model (refs. 13, 14). For this investigation, Freon-12 at a nominal density of .006 slug/ft^3 was used as the test medium.

Model Description

The experimental blades described herein were tested on the aeroelastic rotor experimental system (ARES) shown in Figures 2 and 3. The ARES has a generalized helicopter fuselage shape enclosing the rotor controls and drive system. It is powered by a variable frequency synchronous motor rated at 47 hp output at 12,000 rpm. The motor is connected to the rotor shaft through a belt-driven two-stage speed reduction system. The ARES rotor control system and pitch attitude (α_s) are remotely controlled from within the wind-tunnel control room. The ARES pitch attitude is varied by an electrically controlled hydraulic actuator. Blade collective pitch and lateral and longitudinal cyclic pitch are input to the rotor through the swashplate. The swashplate is moved by three hydraulic actuators.

[1]Freon-12: Registered trademark of E.I. du Pont de Nemours & Co., Inc.

Description of Rotor Blades

The rotor models used in this investigation were 0.175-scale, four-blade articulated rotors with coincident lead-lag, and flapping hinges. The blade geometry was the same for both rotors tested (Figure 4). The blades were designed so that the tip configuration could be changed at the 89 percent radius. The rotor planform was a 0.175-scale representation of a current full-scale utility-class rotor system. An SC1095 airfoil was used on all blades from the root cutout to 49 percent radius and from 91 percent radius to the tip. Between 50 and 90 percent radius, a cambered SC1095-R8 airfoil was used. Adjustable trailing edge tabs of 6.5 percent chord were provided on both sets of baseline and ACR blades from 50 to 89 percent radius.

The baseline blades were aeroelastically representative, but blade structural and inertial characteristics did not precisely match any specific full-scale rotor. The ACR blades differed significantly from the baseline blades in torsional stiffness over the outer 55 percent of the blade span. The blade physical properties and the natural frequencies are presented in Table I.

Instrumentation

Instrumentation on the ARES allows continuous displays of model control settings, rotor forces and moments, blade loads, and pitch link loads. ARES pitch attitude is measured by an accelerometer, and rotor control positions are measured by linear potentiometers connected to the swashplate. Rotor blade flapping and lagging are measured by rotary potentiometers mounted on the rotor hub and geared to the blade cuff. Rotor shaft speed is determined by a magnetic sensor. One blade of each blade set, baseline and ACR, was instrumented with four-arm strain-gage bridges to measure loads and deflections at several blade radial stations. Flapwise (out-of-plane) moments and chordwise (in-plane) moments were measured at 26, 39, 53 and 81 percent radius, while torsional moments were measured at 29, 37, 52, and 78 percent radius. The rotating blade data are transferred through a 30-channel slip-ring assembly. Rotor forces and moments are measured by a six-component strain-gage balance mounted below the pylon and drive system. The balance is fixed with respect to the rotor shaft and pitches with the fuselage. Fuselage forces and moments are not measured by the balance.

Description of Parametric Tips

Seven blade tip designs were evaluated on the baseline rotor and six of the tip designs were tested on the torsionally soft (ACR) blades. The tip designs incorporated a systematic variation in geometric parameters including sweep, taper, and anhedral. These parameters were varied while tip inertial properties, airfoil contour, and twist were target constants. The magnitude of parameter variations chosen for ACR application were representative of current design values for modern helicopter rotors. Figure 5 presents the geometry of the tip designs, while Table II lists the measured tip characteristics and compares them to the design goals or controlled constants.

Test Methodology

Procedure for Performance and Loads Data Acquisition

Each rotor configuration was first tracked and balanced in hover to remove first harmonic fixed system loads. At each forward flight test point, the rotor rotational speed and tunnel conditions were adjusted to give the desired tip Mach number and advance ratio at a given shaft angle of attack. Blade collective pitch was changed to obtain the target rotor lift and propulsive force; and at each collective pitch setting, the cyclic pitch was used to remove rotor first-harmonic flapping with respect to the rotor shaft. Data were then recorded for each rotor task. The maximum value of collective pitch attained at each shaft angle of attack was generally determined by either blade load limits or ARES drive system limits.

Model deadweight tares were determined throughout the shaft angle of attack range with the blades on and with them removed. Aerodynamic rotor hub tares were determined with the blades removed throughout the ranges of shaft angle of attack and advance ratio investigated. Both deadweight and hub aerodynamic tares have been removed from the data presented herein.

Procedure for Rotor Track Sensitivity Data Acquisition

For the configurations tested for tracking characteristics, the procedure for tracked rotor data was similar to that above. During out-of-track conditions the instrumented blade was driven out of track with trailing edge tab deflections, and allowed to fly out of trim with the shaft. Flapping for the remaining three blades had first-harmonic content removed through cyclic pitch.

Accuracies

Based on controlled data points, the repeatability of the data for constant shaft angle of attack, control angles and advance ratio has been estimated to be within the following limits.

$$\frac{C_L}{\sigma} \pm 0.0025$$

$$\frac{C_D}{\sigma} \pm .0005$$

$$\frac{C_Q}{\sigma} \pm .00025$$

The accuracy for angle measurements is estimated to be within $\pm 0.25°$.

The value of solidity (σ) used throughout this report for normalizing performance coefficients is 0.082, based on a blade nominal chord of 3.625 inches and a radius of 56.224 inches.

Test Conditions

Data Obtained

All the tip configurations shown in Figure 5 were tested for the target conditions shown in Table III. The magnitudes of lift and propulsive force parameters and advance ratio were chosen as representative of a modern utility helicopter. The tip Mach number variation represents that possible due to full scale ambient environment changes and also represents an attempt to evaluate the effect of changes in advancing tip Mach number on the tip airfoil and planform behavior.

The ACR and baseline rotors with swept tips were subjected to a rotor track sensitivity study which included the target test points shown in Table IV.

Data for Analysis

Within the scope of this paper, the performance and loads data presented for analysis emphasizes the target lift and propulsive force parameters of Table III, but is limited to one rotational tip Mach number (0.65), and two advance ratios (0.35 and 0.40). The exception to this is the rotor track sensitivity data analysis which includes advance ratios of 0.20, 0.30, and 0.40.

Results

Rotor Performance

Fixed system forces and torque were obtained using the procedures and limits described earlier for all tip configurations for the test conditions listed in Table III. Parametric performance results for selected conditions are presented in Figure 6. The advance ratios and lift parameter, $C_{L/\sigma}$, conditions were selected for presentation because they showed the most significant difference in rotor performance between configurations. Below an advance ratio of .30, rotor performance differences were smaller for a given task.

The parametric effect of tip shape on rotor performance for the complete set of tips is shown in Figure 7. These diagrams present the percent reduction or increase in torque coefficient for a given rotor task for each tip shape. This method of presentation of rotor performance allows the separation of parametric geometry effects to be easily quantified. As an example, for the baseline blades tested and the conditions shown, the rotor's performance was enhanced by the addition of anhedral to a rectangular planform and the addition of sweep to the tapered planform. Tip taper improved rotor performance at μ = .35 conditions but not at higher speeds (μ = .40). Figure 6 shows that although tip configuration changes had measurable performance effects on torsionally soft and stiff blades, higher torque requirements were shown for the conformable rotor applications.

Rotor Loads

Blade oscillatory loads are important not only from vibratory fatigue considerations but also because they provide insight into the blade loading environment and elastic deformation trends. Torsional loads and flapwise oscillatory loads are associated with local blade loading and twist (ref. 8). Figure 8 presents 1/2 peak-to-peak flapwise loads at 4 spanwise stations for the configurations tested. These oscillatory loads are data points taken at the μ, M_T, $C_{L/\sigma}$ and α_s values listed for each tip configuration. The configurations are also ranked in Figure 8 according to their performance at the $C_{D/\sigma}$ values shown. Examination of Figure 8 shows a configuration variance in flapwise loads at each test condition as well as a significant relationship between performance and oscillatory flapwise loads. Specifically, the configurations which exhibited the lowest flapwise loads had the best performance characteristics while the poor performance configurations had the highest flapwise loads.

Elastic Twist

Spanwise distributions of blade torsional moment time histories were converted to elastic twist distributions through measured blade torsional stiffness properties. The deflections are shown in Figure 9 for all configurations tested at the μ, M_T, $C_{L/\sigma}$ and α_s values listed. Some interpolation of the inboard torsional loads occasionally was necessary. The elastic twist is configuration dependent for each rotor task and condition and, as might be expected, varies with rotor environment. The elastic twist waveforms are comprised of several harmonics, but are dominated by the one per rev torsional component.

The amount of azimuthal activity in the elastic twist plots is of interest, especially when it is compared with the integrated rotor performance for each configuration. The figure 9 waveforms have, in fact, been arranged in order according to each configuration's torque coefficient for the rotor tasks shown with the lowest torque configuration appearing first, and the highest torque configuration last in each case. A correlation between rotor performance and elastic twist is evident in the data shown. Specifically, the configurations which exhibited small aziumthal activity in elastic twist were the best performers.

Analysis of Results

General

The performance and loads data for the baseline and ACR configurations were examined to provide insight into the mechanism by which the tip planform and torsional stiffness parameters affected the aeroelastic behavior of the rotor blades. The designed differences between configurations were evaluated for the

fundamental changes they caused in the rotor's performance and response in light of past and current conformable design concepts, for example, elastic twist. Rigid blade analyses have been employed on this data (ref. 12). Although tip solidity effects on rotor performance were predicted fairly well using a non-uniform inflow analysis, the effects of certain tip parameters, such as anhedral, were inadequately predicted with regard to performance trends.

Blade Elastic Twist Magnitude

Past conformable rotor design concepts have considered the magnitude of advancing blade elastic twist as a solution to a potentially unfavorable angle of attack environment (ref. 2, for example). Depending on the tip airfoil section and advancing blade Mach number, a nose-up elastic twist was thought to be desirable to achieve lower rotor torque and blade loads. Figure 10 presents elastic twist magnitudes on the advancing side (ψ = 90°) for each configuration and rotor task shown. Figure 10 also contains the total geometric pitch angle for the above conditions, which is comprised of elastic twist, built-in twist, collective and cyclic pitch angles at ψ = 90°. Both types of blade angle data are also ranked according to their configuration's performance.

As is evident from Figure 10, there is no strong correlation between the magnitude of each configuration's advancing blade elastic or total pitch angle and the performance of the rotor. It is recognized that configuration performance and loads depend on local angle of attack which is affected by inflow distribution as well as pitch angle and that non-uniform inflow velocity can be very sensitive to planform configuration. Nevertheless, the design of a conformable rotor has received attention for achieving specific azimuthal placement of elastic twist magnitudes. The present studies do not support this as an ACR design goal.

Conformable Rotor Control

Conformable rotors which experience significant blade torsional response may generate rotor control characteristics which should be evaluated for their contributions to rotor stability and control (ref.8). Throughout the test program described herein, all configurations were easily controlled through the model actuator-swashplate system for all test conditions. The amount of control needed to achieve each rotor task was configuration dependent however, especially when comparing the torsionally soft rotor tip configurations with their corresponding baseline counterparts. Figure 11 shows, for a representative rotor task, the longitudinal cyclic pitch required to remove first harmonic flapping with respect to the rotor shaft for several configurations which differ in blade torsional stiffness.

The differences in longitudinal cyclic pitch for these configurations is significant not so much for control travel considerations, but for what these angles reveal about the rotor behavior for these tip shapes and torsional stiffnesses. Specifically, the differences in elastic twist measured for several configurations, shown in Figure 11a-c are offset by control input differences of nearly the same magnitude in order to remove the first harmonic flapping with respect to the rotor shaft. There were exceptions to this trend, notably for the swept tip (Figure 11d).

Another interesting connection was observed in both the pitch control required to trim the rotor and the rotor task achieved, in particular, the rotor propulsive force. For a given advance ratio, tip Mach number, force normal to the trimmed tip path plane, and shaft angle of attack, the torsionally soft rotor configurations consistently exhibit more positive rotor drag. This can be seen in the performance data of Figure 6. Examination of the rotor balance forces reveals that this increase in rotor drag occurs for two primary reasons. First, the control axis for the torsionally soft rotor has tilted aft due to the changes in longitudinal pitch mentioned above. Secondly, the rotor longitudinal force perpendicular to the control axis (H-force) is greater for the torsionally soft blade. The control axis aft-tilt is due to the test methodology used and the nose-down elastic twist magnitude observed. The H-force increase for the ACR configurations is probably due to integrated drag loading increases around the azimuth. This would also manifest itself in decreased rotor efficiency, a fact which was shown earlier in this paper for these configurations (Figure 6).

Blade Loading

It is well known that the radial and azimuthal distribution of rotor blade loading can affect both performance and loads. The potential of the conformable rotor concept to tailor these airloads has, in fact, been viewed as a key to the optimization of rotor performance (ref. 2). Specifically, a redistribution of airloads which avoids sharp radial and azimuthal gradients in loading and generates airload symmetry has been investigated for rotor performance improvement (ref. 15).

As previously shown, the rotor configurations described in this paper which exhibited good performance and low vibratory loads generated the least activity in elastic twist around the azimuth. Because several configurations provided significant aerodynamic center-elastic axis offsets, the elastic twist variations observed may be primarily due to oscillatory tip lift. Although section pitching moment variations may add to elastic twist perturbations around the azimuth, these would also be lift dependent.

It is therefore possible that the success of those configurations which exhibited low vibratory loads and increased performance is based on a redistribution of lift either radially or azimuthally, or both. This is reinforced by the previously mentioned rigid

blade analytical results (ref. 12) which correctly predicted no marked performance variations due to the small solidity differences between configurations. The cause of the apparent airload redistribution may be found in the parameter combinations which complement each other. For example, as has been shown previously in Figure 7, anhedral seems to aeroelastically help a baseline blade rectangular tip planform more that it does a swept-tapered planform. Furthermore, the addition of sweep for the baseline blade seems to enhance the aerodynamic environment of a tapered planform more than it does a rectangular tip for the configurations tested. The use of an aeroelastic analysis would be necessary to quantify this observation, but the test results included herein encourage this loading hypothesis.

Conformable Rotor Track Characteristics

General

The utilization of a conformable rotor concept should be evaluated not only for the measure of success with which it achieves its performance and loads goals, but also how well it can be "fielded." That is, how much change (if any) in current installation, maintenance, and rotor tuning is necessary for the new rotor concept to be employed. One aspect of this transition is rotor tracking sensitivity and its implications for rotor and fuselage loads.

Because the results of this study and others have indicated that the response of torsionally soft rotors to parametric changes can be significant, a track sensitivity study was initiated in which baseline and ACR blades with representative swept tips were subjected to a test matrix (Table IV) designed to perturb the track of one blade in the rotor. The perturbation was accomplished by use of trailing edge tab deflection. Specifically, the outermost two tabs (85-89 percent radius) were deflected 4 degrees down on the instrumented blade.

The use of trailing edge tabs for conformable rotor use has been described in ref. 8 for performance and ref. 16 for vibration. The use of trailing edge tabs in this study was for tracking sensitivity. Initially the tabs were undeflected and the rotor tracked in hover. One-per-rev longitudinal and lateral fixed-system loads were minimized through standard balance techniques. The rotors were then subjected to the forward flight conditions of Table IV. The forward flight process was then repeated for the deflected tabs and data acquired until either the test matrix was completed or loads became prohibitive.

Blade Torsion Due to Tab Deflection

The torsional blade loads are shown in Figure 12 for the tracking conditions. The data was chosen at a blade station just inboard of the deflected tab locations. The 0° tab cases show ACR mean nose-down moments greater than the baseline. The differences in loads would be expected to result in mean elastic twist differences similar to the trends observed earlier in this paper. The addition of tab deflection produces more nose down torsional moment for the ACR.

The oscillatory torsional moment of the ACR is comparable to the baseline rotor for 0° tab deflection, but is more sensitive to tab deflection than the baseline rotor's torsional load (Figure 12 c,d). The elastic twist resulting from these load perturbations would be expected to change the track and vibration characteristics of these rotors.

Blade Flapping Due to Tab Deflection

The flapping response of the instrumented blade to tab deflection is shown in Figure 13 for both rotors. As mentioned previously, the other three blades of each rotor were trimmed to the rotor shaft for all conditions, so that the flapping of the instrumented blade, above the mean coning, is a measure of out-of-track sensitivity.

The ACR coning for both 0° tab and 4° tab shows the effect of large mean elastic twist for this rotor as well as the increased sensitivity to tab deflection. The baseline rotor exhibits, as expected, less mean elastic twist, and hence, less effect on coning. The one-per-rev flapping (Figure 13 c,d) for the ACR blade shows a large (3.5 degrees) out-of-track sensitivity due to tab deflection, compared to that of the baseline. This phenomenon may also be due to the large ACR oscillatory elastic twist produced by tab deflection.

Flapwise Blade Loads Due to Tab Deflection

The effect of elastic twist changes to inboard blade loading is of interest for blade life and fixed system vibratory loads implications. Figure 14 shows the effect of blade configuration and tab deflection on the inboard flap loading. As might be expected from the steady elastic twist and coning data shown previously, the ACR loading shifts inboard with tab deflection and the mean inboard flapwise moment sharply drops.

In like manner Figure 14 c,d shows the effect of oscillatory elastic twist, caused by tab deflection, on the oscillatory flapwise loads for both rotors. The ACR flapwise moment appears more sensitive to tab deflection than that of the baseline rotor. These loads should manifest themselves in fixed-system vibrations as discussed in the next section.

Fixed System Vibrations Due to Tab Deflection

The blade torsional response to a parameter change such as tab deflection has thus been shown to affect blade track and blade loads. Both blade track and loads are transferred to the fixed system, an obvious practical consideration to the vibration of the helicopter during tracking procedures. Figure 15 shows that the one-per-rev vertical load in the fixed system is much more sensitive to the 4 degree tab deflection for the

torsionally soft rotor than for the baseline. This was also observed (but not shown herein) for the fixed system in-plane loads. It is also interesting that the undeflected tab configuration for the ACR produced more fixed system one-per-rev vertical loading than the baseline. This occurred even though the ACR inboard oscillatory flapwise load for 0° tab was only slightly greater than the baseline's.

Although the reduced torsional stiffness of the ACR affords greater torsional deflection for a given tab input, the implied increase in tracking capability should be weighed against the above results. These results indicate a potential coupling of blade torsional deflection, blade oscillatory loads, and fixed system vibration which results from a high sensitivity of the conformable rotor to practical tracking procedures.

Conclusions

Based on the data obtained for the test conditions and model configurations investigated, the following conclusions have been reached:

1. Significant performance and loads differences were generated by tip geometry variations.

2. Torsionally soft rotor (ACR) applications for the tip shapes tested resulted in substantially different performance and loads than for the baseline configuration.

3. Elastic torsional deflection varied with tip shape and operating conditions for both the baseline blade and the torsionally soft blade.

4. There exists a strong correlation between azimuthal variation of elastic twist and rotor performance and loads.

5. There does not exist a strong correlation of advancing blade elastic twist magnitude with rotor performance or loads.

6. Fixed system vibratory loads and rotor track for potential ACR candidates appear very sensitive to parametric rotor changes.

References

1. Doman, Glidden S.; Tarzanin, Frank J.; and Shaw, John, Jr.: Investigation of Aeroelastically Adaptive Rotor Systems. Proceedings of a Symposium on Rotor Technology, American Helicopter Society, August 1976.

2. Blackwell, R. H.; and Merkley, D. J.: The Aeroelastically Conformable Rotor Concept. Preprint No. 78-59. American Helicopter Society, May 1978.

3. Berry, John D.; and Mineck, Raymond E.: Wind-Tunnel Test of an Articulated Helicopter Rotor Model With Several Tip Shapes. NASA TM 80080, 1980.

4. Stroub, Robert H.; Rabbott, John P., Jr.; and Niebanck, Charles F.: Rotor Blade Tip Shape Effects on Performance and Loads From Full-Scale Wind-Tunnel Testing. Journal of the American Helicopter Society, Volume 24, No. 5, October 1979, pp. 28-35.

5. Philippe, J. J.; and Vuillet, A.: Aerodynamic Design of Advanced Rotors with New Tip Shapes. 39th Annual Forum Proceedings, American Helicopter Society, May 1983.

6. Weller, William H.: Experimental Investigation of Effects of Blade Tip Geometry on Loads and Performance for an Articulated Rotor System. NASA TP 1303, 1979.

7. Sutton, Lawrence R.; White, Richard P., Jr.; and Marker, Robert L.: Wind-Tunnel Evaluation of an Aeroelastically Conformable Rotor. USAAVRADCOM-TR-81-D-43, 1982.

8. Blackwell, R. H.; Murrill, R. J.; Yeager, W. T., Jr.; and Mirick, P. H.: Wind-Tunnel Evaluation of Aeroelastically Conformable Rotors. Preprint No. 80-23, 36th Annual Forum Proceedings, American Helicopter Society, May 1980.

9. Yeager, William T., Jr.; and Mantay, Wayne R.: Wind-Tunnel Investigation of the Effects of Blade Tip Geometry on the Interaction of Torsional Loads and Performance for an Articulated Helicopter Rotor. NASA TP 1926, 1981.

10. Yeager, William T., Jr.; and Mantay, Wayne R.: Loads and Performance Data From a Wind-Tunnel Test of Model Articulated Helicopter Rotors with Two Different Blade Torsional Stiffnesses. NASA TM 84573, 1983.

11. Blackwell, R. H.; and Frederickson, K. C.: Wind-Tunnel Evaluation of Aeroelastically Conformable Rotors. USAAVRADCOM-TR-80-D-32, 1981.

12. Mantay, Wayne R.; and Yeager, William T., Jr.: Parametric Tip Effects for Conformable Rotor Applications. NASA TM 85682, 1983.

13. Lee, Charles: Weight Considerations in Dynamically Similar Model Rotor Design. SAWE Paper No. 659, May 1968.

14. Hunt, G. K.: Similarity Requirements for Aeroelastic Models of Helicopter Rotors. C. P. 1245, Royal Aircraft Establishment, 1973.

15. Moffitt, Robert C.; and Bissell, John R.: Theory and Application of Optimum Airloads to Rotors in Hover and Forward Flight. 39th Annual Forum Proceedings, American Helicopter Society, May 1982.

16. Kottapalli, S. B. R.: Hub Loads Reduction by Modification of Blade Torsional Response. 39th Annual Forum Proceedings, American Helicopter Society, May 1983.

TABLE IA. Model Blade Properties

Baseline Blade

INBOARD SECTION r/R	SECTION LENGTH (ft)	SECTION MASS (slugs)	STIFFNESS ($lb\text{-}ft^2$) FLAP	CHORD	TORSION	I_θ ($lb\text{-}sec^2$) $X10^{-3}$
.0534	.322	.051	101,944.	104,166.7	6,763.9	.57
.1222	.166	.011	9,326.4	69,444.4	1,269.6	.143
.1577	.333	.0062	9,326.4	2,777.8	432.1	.05
.2288	.333	.0062	74.3	2,777.8	236.1	.05
.2999	.333	.0062	74.3	2,777.8	88.9	.05
.371	.333	.0062	74.3	2,777.8	88.9	.08
.4421	.333	.0062	81.3	2,777.8	91.6	.08
.5132	.333	.0062	75.7	2,777.8	93.1	.08
.5843	.333	.0062	81.3	2,777.8	94.4	.08
.6554	.333	.0062	81.3	2,777.8	94.4	.08
.7265	.333	.0062	81.3	2,777.8	94.4	.08
.7976	.333	.0062	86.8	2,777.8	92.4	.08
.8687	.207	.0054	33.3	694.4	95.4	.117
.9128	.073	.0024	33.3	694.4	27.1	.117
.9283	.336	.0045	21.5	347.2	22.0	.117

Rotating Natural Frequencies at Ω = 68.07 rad/sec

MODE	ω/Ω
Flap	2.68
Flap	4.98
Chord	5.08
Torsion	6.14
Flap	8.17

TABLE IB. Model Blade Properties

ACR Blade

INBOARD SECTION r/R	SECTION LENGTH (ft)	SECTION MASS (slugs)	STIFFNESS ($lb\text{-}ft^2$) FLAP	CHORD	TORSION	I_θ ($lb\text{-}sec^2$) X10^{-3}
.0534	.322	.05111	102,083.3	104,166.7	6,763.9	.57
.1222	.166	.0111	9,326.4	69,444.4	1,269.6	.143
.1577	.333	.00618	9,326.4	2,777.8	432.1	.05
.2288	.333	.00616	75.7	2,777.8	230.7	.05
.2999	.333	.00616	75.7	2,777.8	85.4	.05
.371	.333	.00612	75.7	2,569.4	85.4	.08
.4421	.333	.0061	78.5	2,569.4	68.6	.08
.5132	.333	.0061	75.0	2,569.4	33.5	.08
.5843	.333	.0061	71.5	2,569.4	24.1	.08
.6554	.333	.0061	71.5	2,569.4	22.9	.08
.7265	.333	.0061	71.5	2,569.4	22.9	.08
.7976	.333	.0061	88.9	2,569.4	26.2	.08
.8687	.207	.0054	59.7	694.4	27.8	.117
.9128	.073	.0024	59.7	694.4	33.3	.117
.9283	.336	.0045	20.8	347.2	22.3	.117

Rotating Natural Frequencies at Ω = 68.07 rad/sec

MODE	ω/Ω
Flap	2.65
Torsion	4.48
Flap	4.93
Chord	4.98
Flap	8.17

Table II. Model Rotor Blade Tip Characteristics

Parameter	Tip c.g. location (in.)		Tip weight (grms)	Tip twist (deg)	c.g.-a.c. / c (pos. c.g. forward)			$I_{1/4c}$ ($ft\text{-}lb\text{-}sec^2$)
Design Target	Chordwise 1.236	Spanwise 2.774	71	1.35	.96R	.98R	1.0R	x 10^{-5} .955R to R
Tip Configuration								
Rectangular	1.30	2.75	73.1	1.27	.028	-.05	.02	.448
Tapered	1.24	2.82	73.4	1.27	-.014	-.056	.007	.197
Swept	1.50	2.85	73.6	1.27	.096	-.04	.019	.56
Swept Tapered	1.31	2.94	71.4	1.27	.096	-.017	.008	.371
Rectangular Anhedral	1.31	2.75	71.1	1.14	.028	-.05	.02	.448
Swept Anhedral	1.48	2.96	70.4	.93	.096	-.04	.019	.56
Swept Tapered Anhedral	1.25	3.00	71.8	1.27	.096	-.017	.008	.371

Rotor Solidity

	Tapered Configurations	Non-tapered Configurations
Area solidity	.08127	.08252
Thrust-weighted solidity	.07905	.08263
Torque weighted solidity	.07793	.08259

Table III. Target Test Conditions

μ	M_T	α_s	$\frac{C_L}{\sigma}$	α_s	$\frac{C_L}{\sigma}$	α_s	$\frac{C_L}{\sigma}$
.30	.65 .68 .70	-6.0°,-7.8° ↓	.06	-4.5°,-5.9° ↓	.08	-3.6°,-4.7° ↓	.10
.35	.65 .67	-8.2°,-10.5° ↓	.06	-6.1°,-7.9° ↓	.08	-4.9°,-6.3° ↓	.10
.40	.63 .65	-10.6°,-13.6° ↓	.06	-8.0°,-10.3° ↓	.08	-6.4°,-8.3° ↓	.10

Table IV. Track Sensitivity Test Conditions

μ	α_s	$\frac{C_L}{\sigma}$	Tab Deflection	M_T
.05 .20 .30 .40	0° 0° -5° -10°	.075 ↓	0°, 4° down ↓	.65 ↓

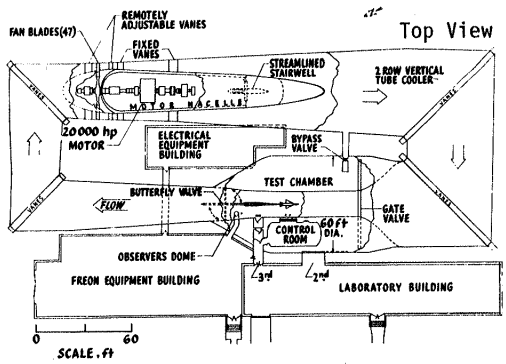

Fig. 1 Langley Transonic Dynamics Tunnel.

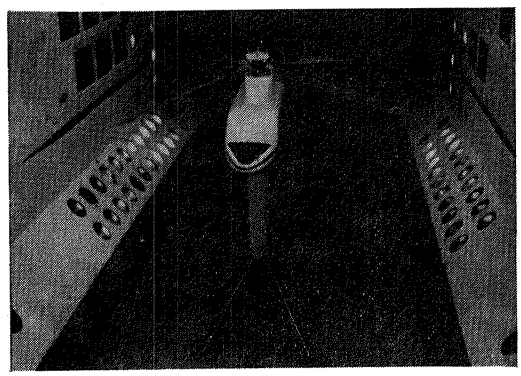

Fig. 2 Aeroelastic rotor experimental system (ARES) model in Langley Transonic Dynamics Tunnel.

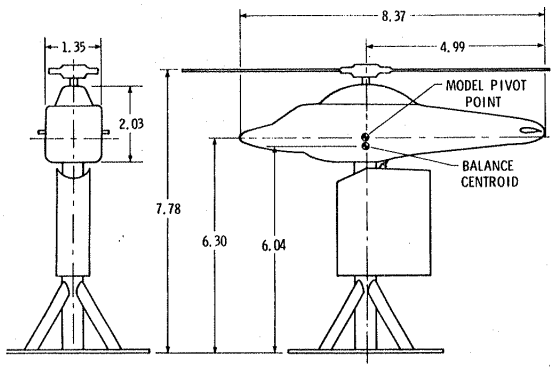

Fig. 3 Schematic diagram of aeroelastic rotor experimental system. All dimensions are in feet.

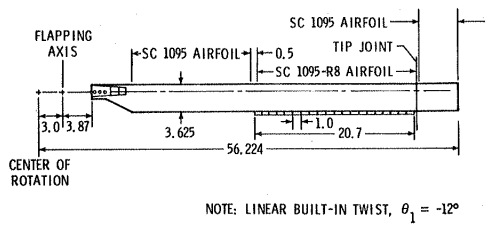

Fig. 4 Rotor blade geometry. Blade dimensions are in inches.

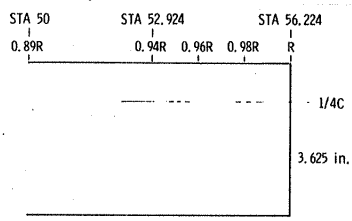

(a) Rectangular

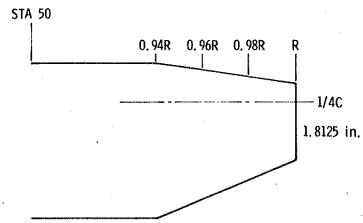

(b) Tapered

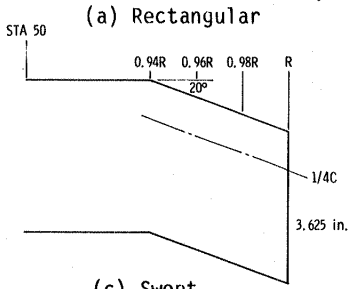

(c) Swept

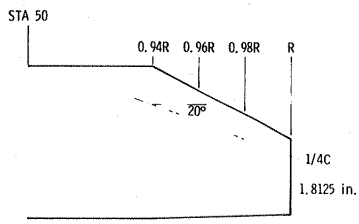

(d) Swept Tapered

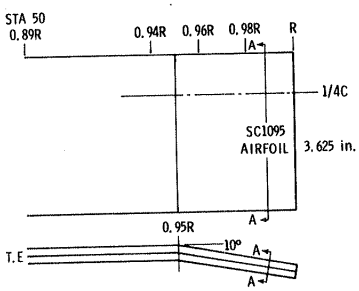

(e) Rectangular Anhedral

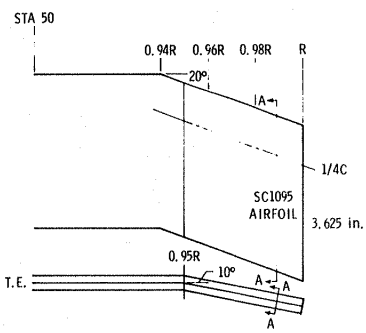

(f) Swept Anhedral

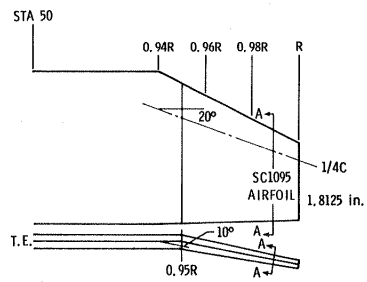

(g) Swept Tapered Anhedral

Fig. 5 Geometry of tips tested. Dimensions are in inches unless otherwise indicated.

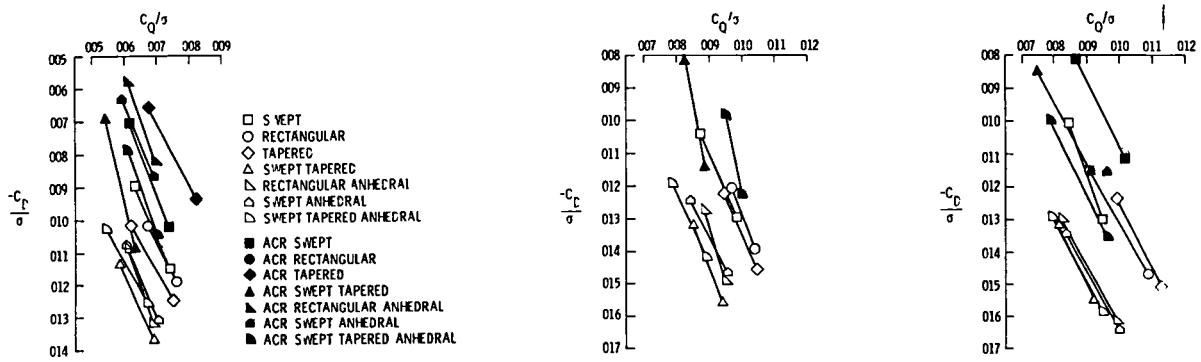

(a)
$\mu = .35$
$M_{TIP} = .65$
$\frac{\overline{C}_L}{\sigma} = .0791$

(b)
$\mu = .35$
$M_{TIP} = .65$
$\frac{\overline{C}_L}{\sigma} = .098$

(c)
$\mu = .40$
$M_{TIP} = .65$
$\frac{\overline{C}_L}{\sigma} = .07885$

Fig. 6 Experimental rotor performance.

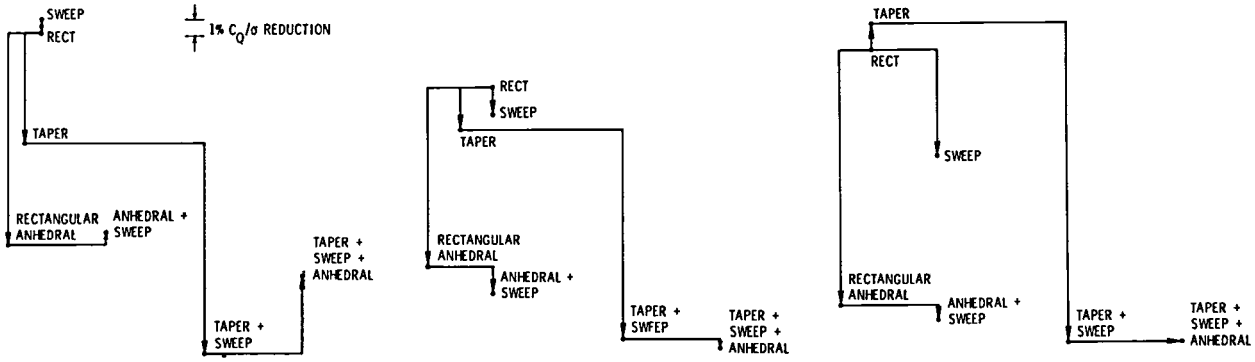

(a)
$\mu = .35$
$M_T = .65$
$\frac{\overline{C}_L}{\sigma} = .07872$
$\frac{C_D}{\sigma} = -.0110$

(b)
$\mu = .35$
$M_T = .65$
$\frac{\overline{C}_L}{\sigma} = .098$
$\frac{C_D}{\sigma} = -.01325$

(c)
$\mu = .40$
$M_T = .65$
$\frac{\overline{C}_L}{\sigma} = .07885$
$\frac{C_D}{\sigma} = -.0145$

Fig. 7 Parametric tip shape effect on experimental baseline rotor performance.

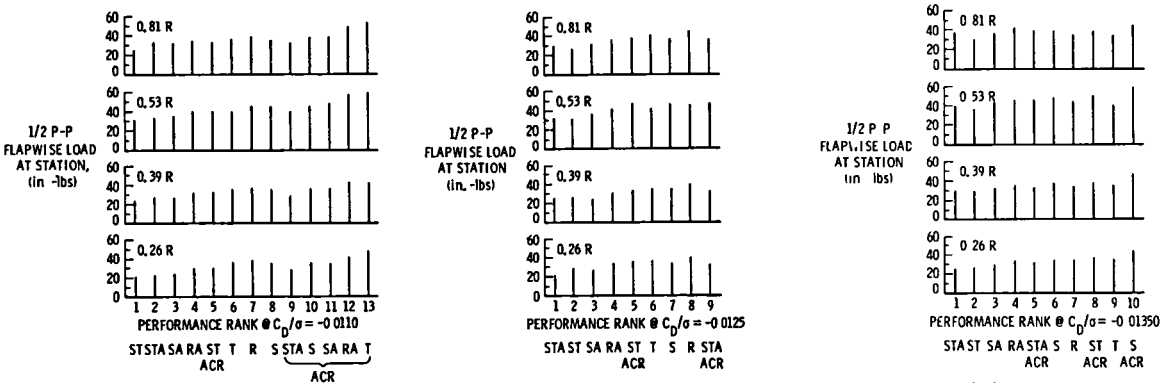

(a)
$\mu = .35$
$M_T = .65$
$\frac{\overline{C}_L}{\sigma} = .0791$
$\alpha_s = -6.1°$

(b)
$\mu = .35$
$M_T = .65$
$\frac{\overline{C}_L}{\sigma} = .098$
$\alpha_s = -4.9°$

(c)
$\mu = .40$
$M_T = .65$
$\frac{\overline{C}_L}{\sigma} = .07885$
$\alpha_s = -8.0°$

Fig. 8 Flapwise oscillatory blade loads versus rotor performance.

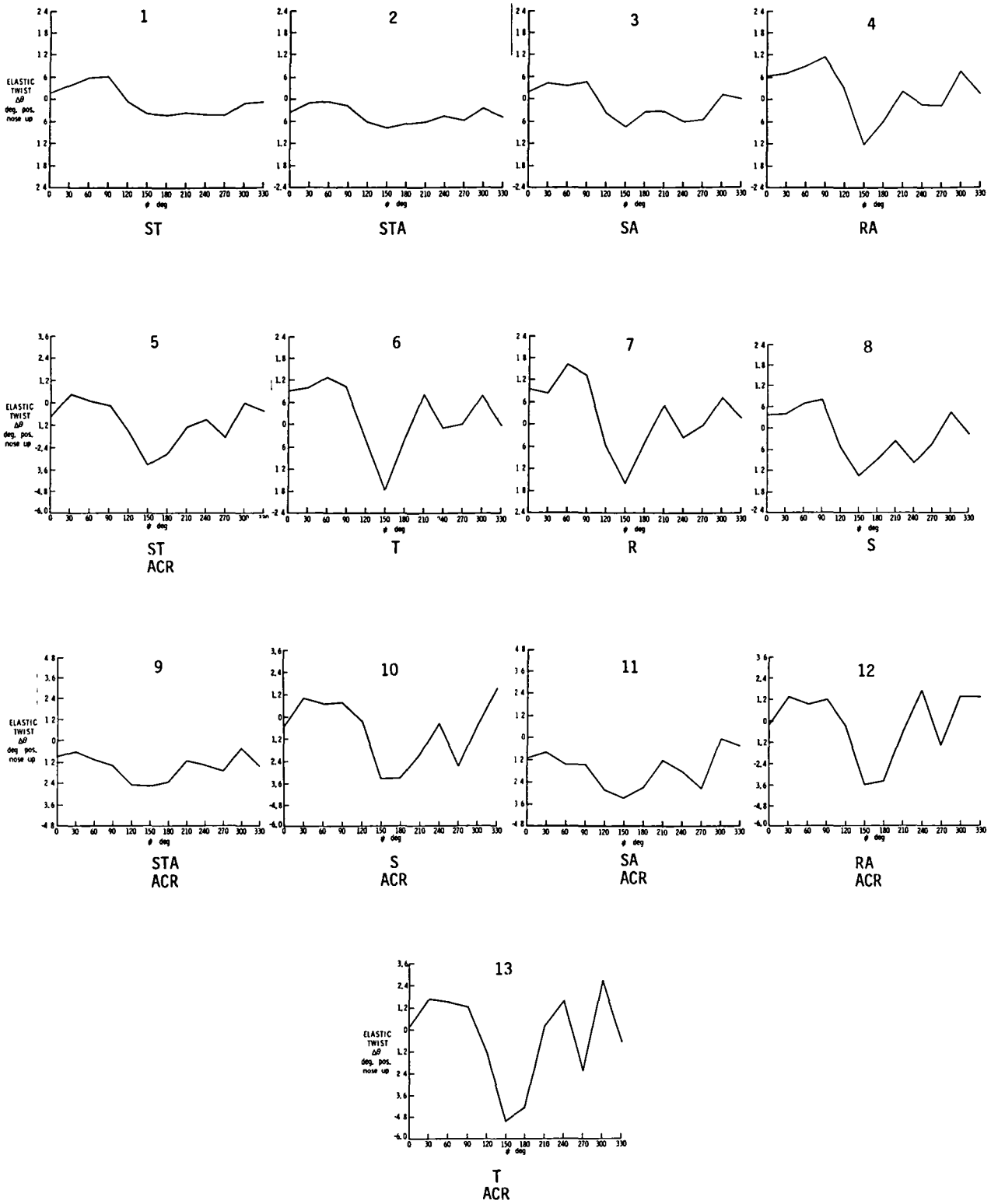

(a) $\mu = .35$, $M_T = .65$, $\frac{C_L}{\sigma} = .0791$, $\alpha_s = -6.1°$. Performance rank at $C_D/\sigma = -.0110$

Fig. 9 Radial distribution of elastic twist versus azimuth at .78R.

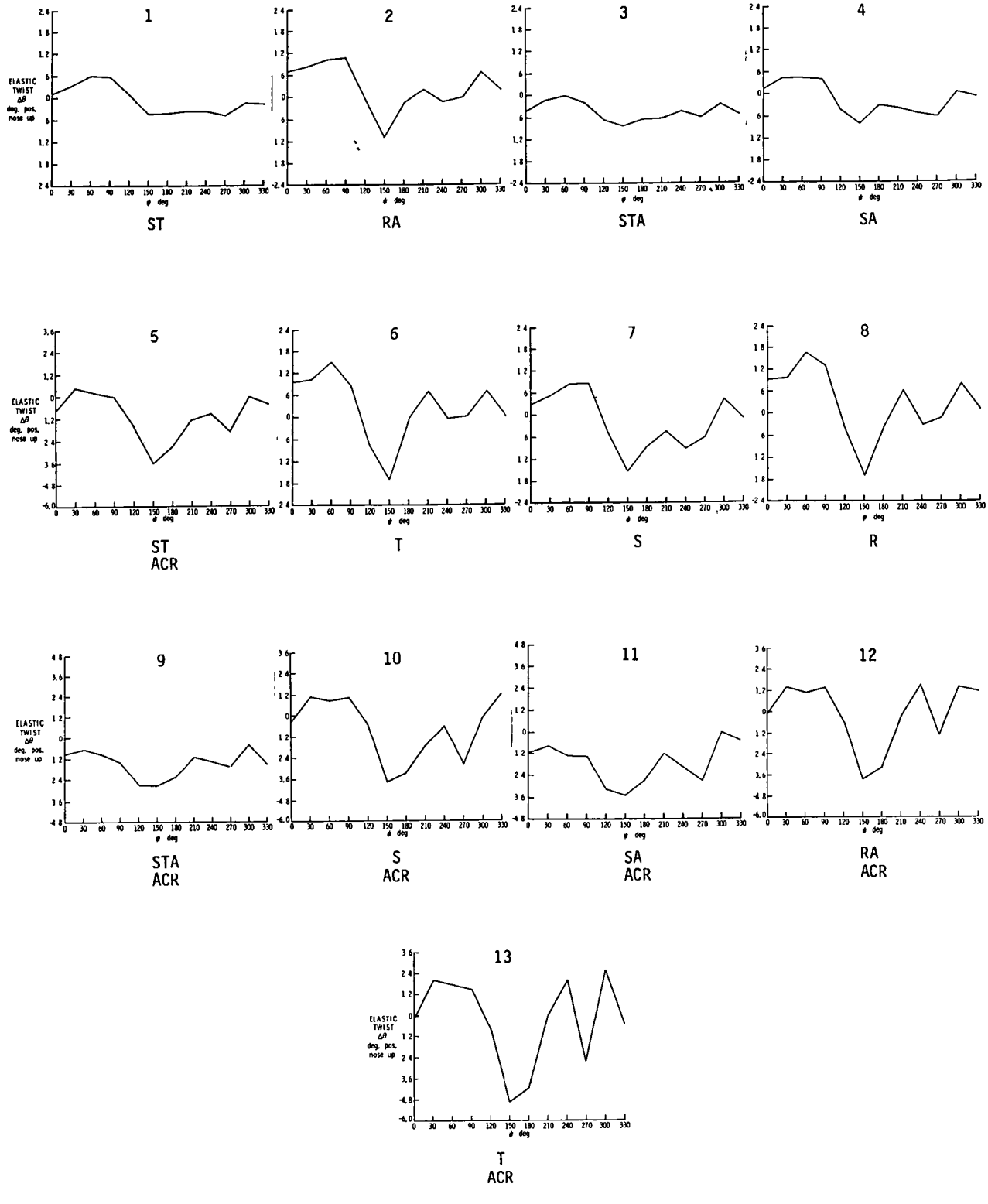

(b) $\mu = .35$, $M_T = .65$, $\frac{\overline{C}_L}{\sigma} = .0791$, $\alpha_s = -7.9°$. Performance rank at $C_D/\sigma = -.01250$

Fig. 9 Continued.

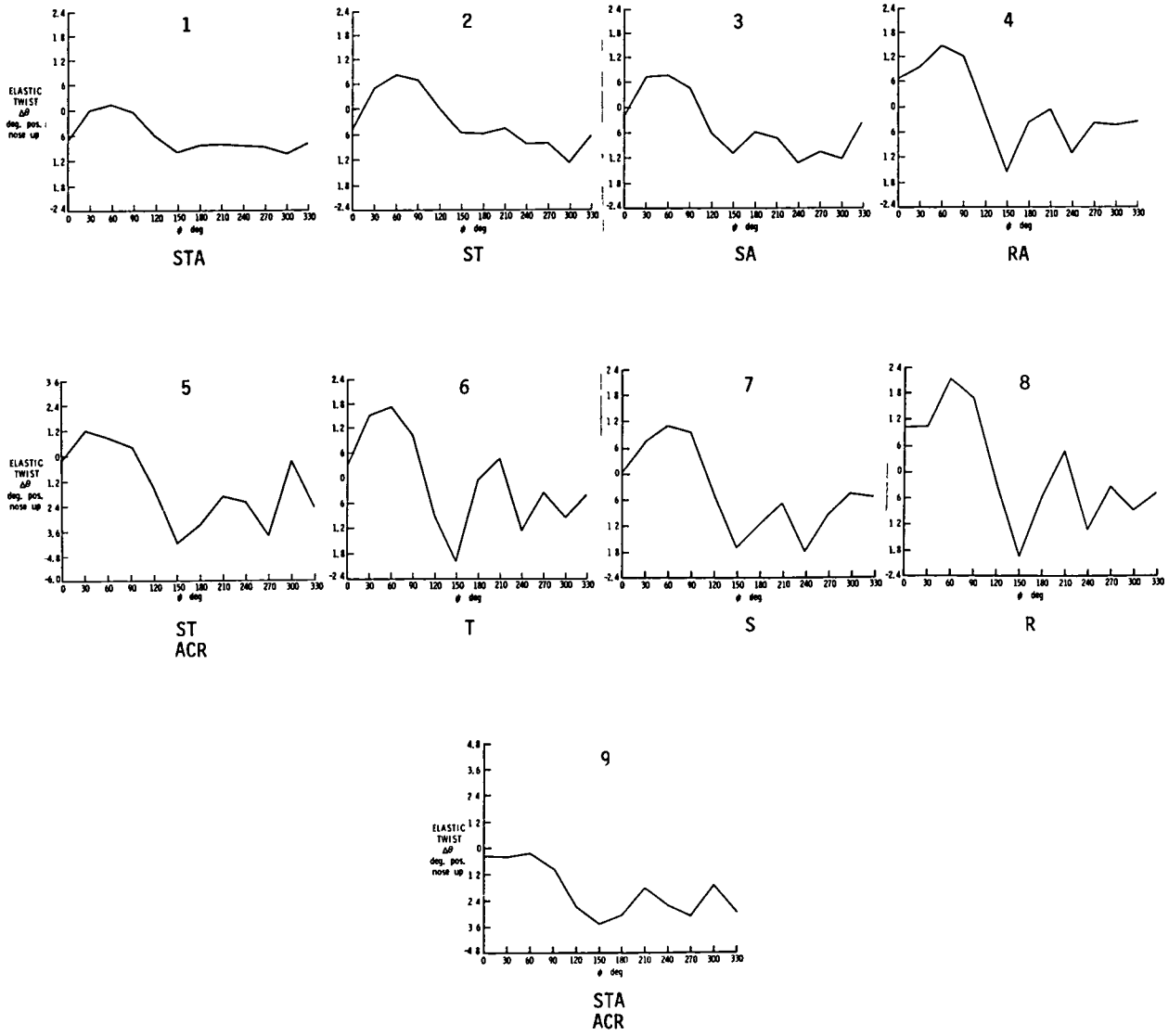

(c) $\mu = .35$, $M_T = .65$, $\frac{C_L}{\sigma} = .098$, $\alpha_s = -4.9°$. Performance rank at $C_D/\sigma = -.0125$

Fig. 9 Continued.

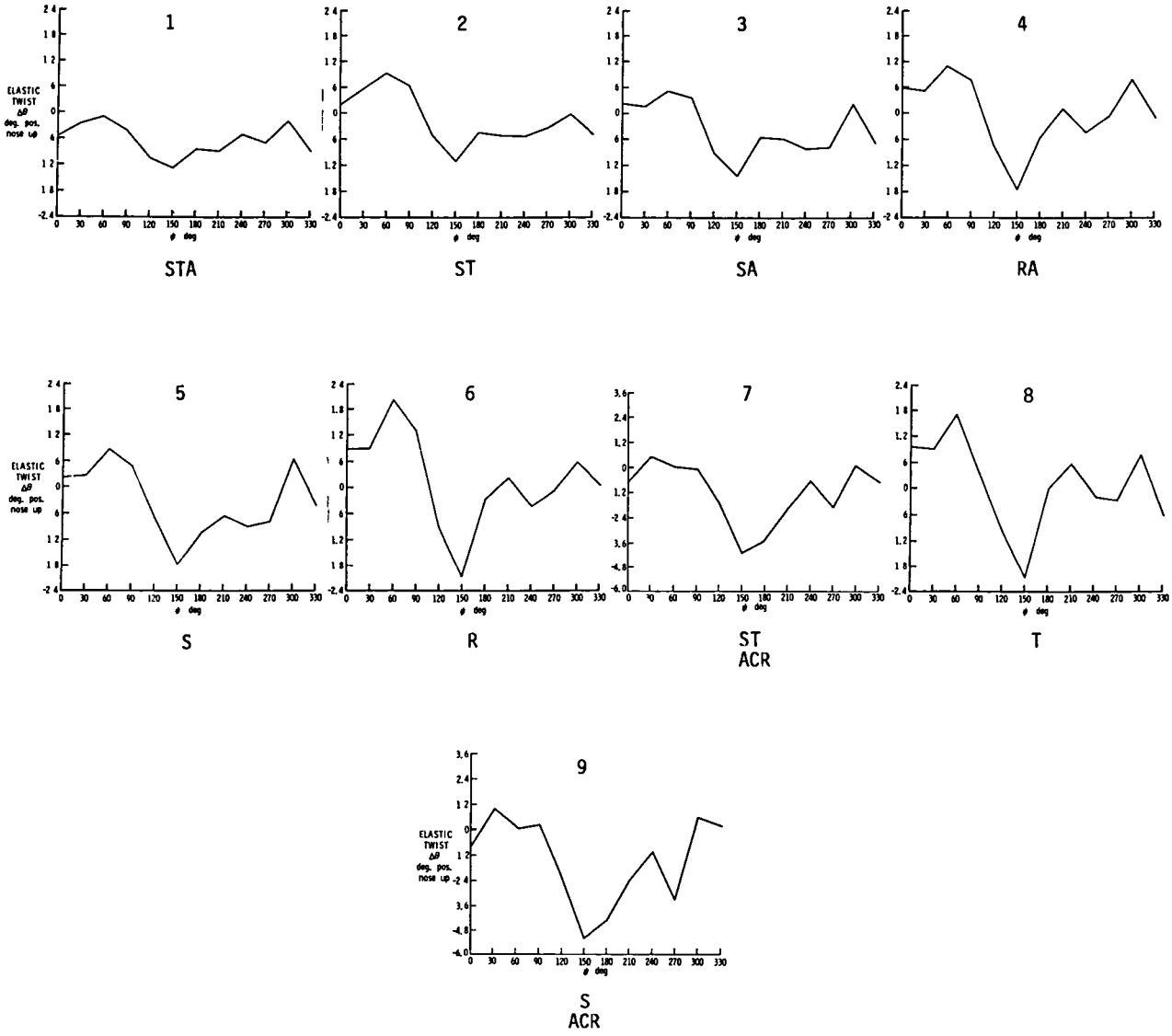

(d) $\mu = .40$, $M_T = .65$, $\frac{\overline{C}_L}{\sigma} = .07885$, $\alpha_s = -8.0°$. Performance rank at $C_D/\sigma = -.01350$

Fig. 9 Concluded.

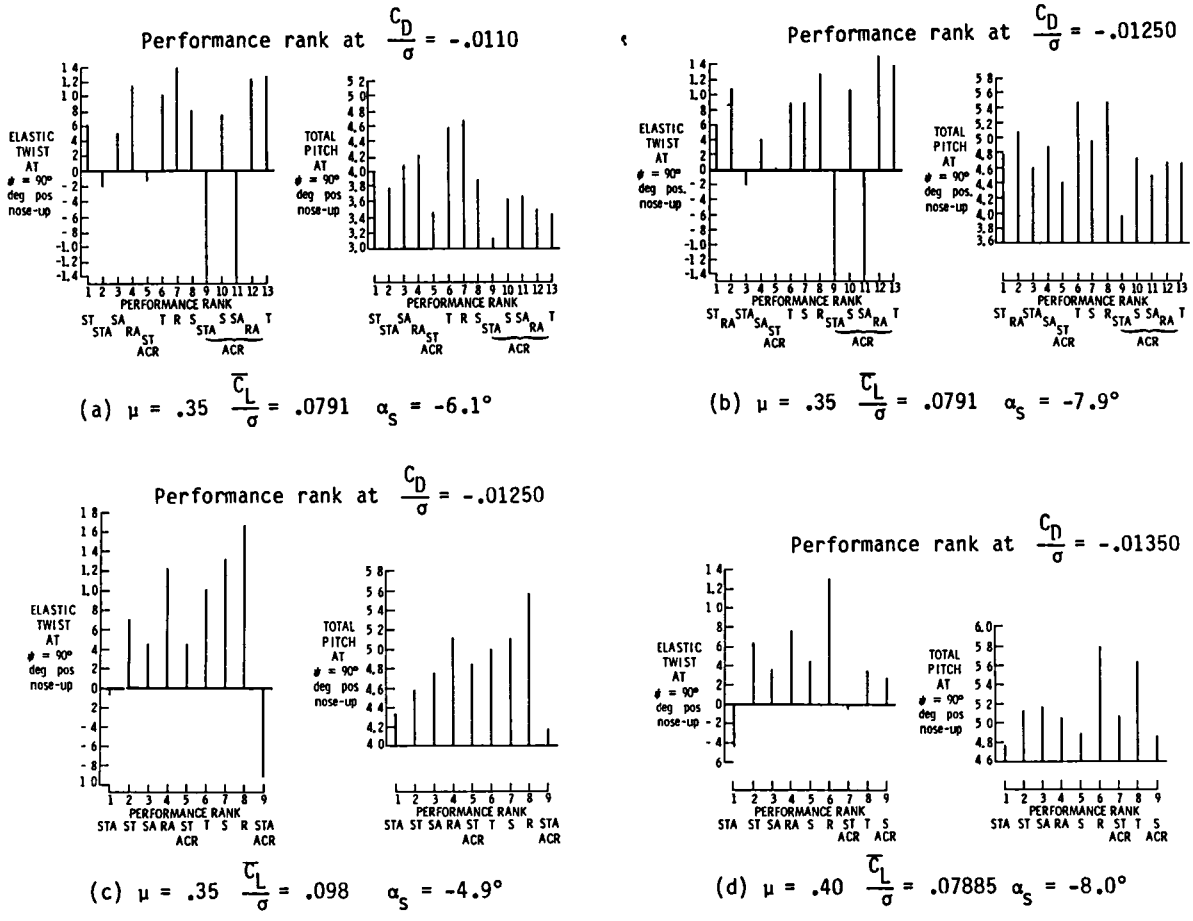

Fig. 10 Advancing side tip elastic twist and total pitch versus configuration performance (r/R = .78 M_T = .65).

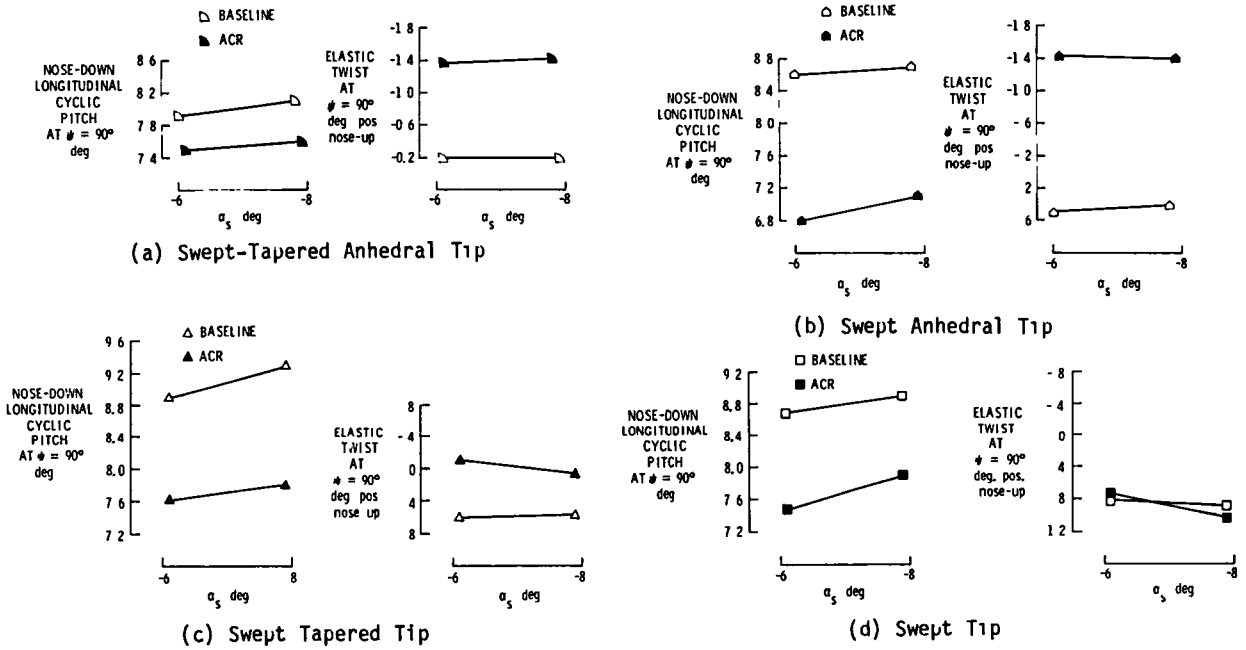

Fig. 11 Advancing blade control angle and elastic twist versus α_S (μ = .35, M_T = .65, $\bar{C}_L/\sigma$ = .08).

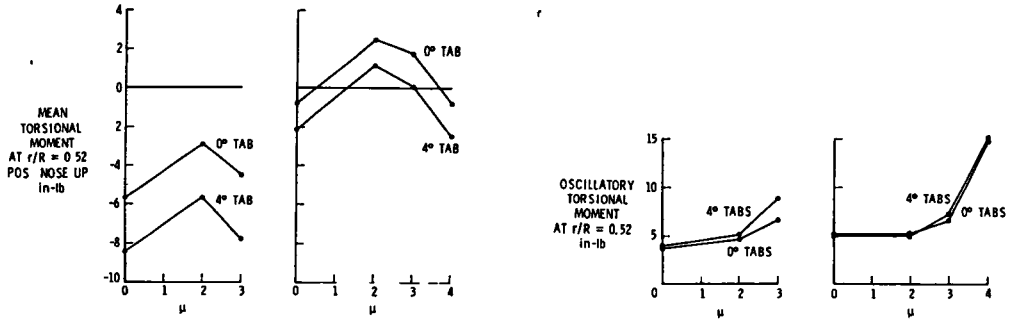

(a) ACR/Swept Tip (b) Baseline/Swept Tip (c) ACR/Swept Tip (d) Baseline/Swept Tip

Fig. 12 Effects of tab deflection on mean and oscillatory outboard torsional moments (M_T = .65, $\frac{\overline{C}_L}{\sigma}$ = 0.075).

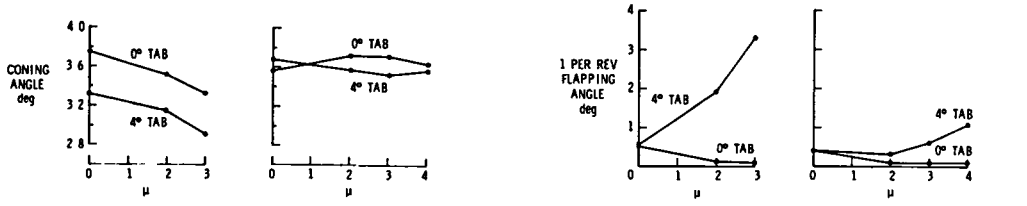

(a) ACR/Swept Tip (b) Baseline/Swept Tip (c) ACR/Swept Tip (d) Baseline/Swept Tip

Fig. 13 Effect of Tab Deflection on Blade Coning and First-Harmonic Flapping Angles (M_T = .65, $\frac{\overline{C}_L}{\sigma}$ = 0.075).

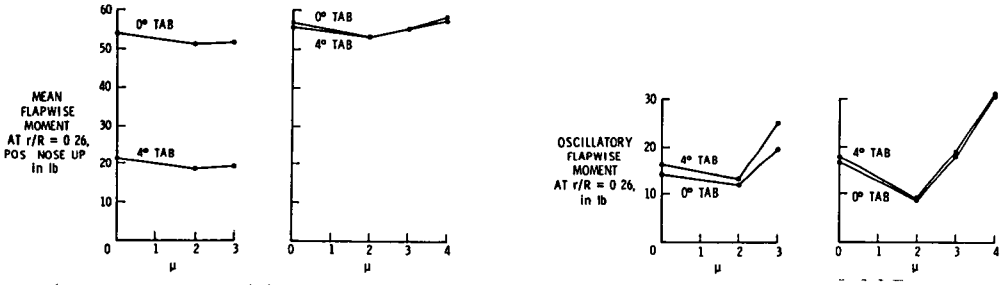

(a) ACR/Swept Tip (b) Baseline/Swept Tip (c) ACR/Swept Tip (d) Baseline/Swept Tip

Fig. 14 Effect of Tab Deflection on Mean and Oscillatory Inboard Flapwise Loads (M_T = .65, $\frac{\overline{C}_L}{\sigma}$ = 0.075).

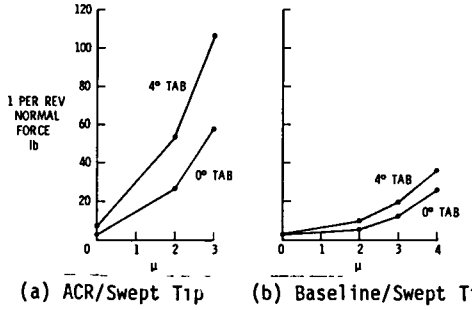

(a) ACR/Swept Tip (b) Baseline/Swept Tip

Fig. 15 Effect of Tab Deflection on Fixed System Normal Loads (M_T= .65, $\frac{\overline{C}_L}{\sigma}$ = 0.075).

Standard Bibliographic Page

1 Report No NASA TM-87687 USAAVSCOM TR-86-B-1	2 Government Accession No.	3 Recipient's Catalog No.
4 Title and Subtitle AEROELASTIC CONSIDERATIONS FOR TORSIONALLY SOFT ROTORS		5 Report Date August 1986 6. Performing Organization Code 505-61-51-03
7. Author(s) Wayne R. Mantay and William T. Yeager, Jr.		8 Performing Organization Report No.
9 Performing Organization Name and Address Aerostructures Directorate AVSCOM Research and Technology Laboratories NASA Langley Research Center Hampton, VA 23665-5225		10. Work Unit No. 11 Contract or Grant No.
12 Sponsoring Agency Name and Address National Aeronautics and Space Administration Washington, DC 20546 & U.S. Army Aviation Systems Command, St. Louis, MO 63166		13 Type of Report and Period Covered Technical Memorandum 14 Sponsoring Agency Code

15. Supplementary Notes

Paper presented at the AHS 2nd Decennial Specialists' Meeting on Rotorcraft Dynamics, November 7-9, 1984, Moffett Field, CA.

16 Abstract

A research study was initiated to systematically determine the impact of selected blade tip geometric parameters on conformable rotor performance and loads characteristics. The model articulated rotors included baseline and torsionally soft blades with interchangeable tips. Seven blade tip designs were evaluated on the baseline rotor and six tip designs were tested on the torsionally soft blades. The designs incorporated a systemmatic variation in geometric parameters including sweep, taper, and anhedral. The rotors were evaluated in the NASA Langley Transonic Dynamics Tunnel at several advance ratios, lift and propulsive force values, and tip Mach numbers. A track sensitivity study was also conducted at several advance ratios for both rotors. Based on the test results, tip parameter variations generated significant rotor performance and loads differences for both baseline and torsionally soft blades. Azimuthal variation of elastic twist generated by variations in the tip parameters strongly correlated with rotor performance and loads, but the magnitude of advancing blade elastic twist did not. In addition, fixed system vibratory loads and rotor track for potential conformable rotor candidates appears very sensitive to parametric rotor changes.

17 Key Words (Suggested by Authors(s))	18 Distribution Statement
Helicopters Wind Tunnel Aeroelasticity	Unclassified - Unlimited Subject Category - 39

19 Security Classif (of this report)	20. Security Classif (of this page)	21. No. of Pages	22. Price
Unclassified	Unclassified	19	A02

For sale by the National Technical Information Service, Springfield, Virginia 22161

End of Document